19

The parton model and QCD

19.1   Introduction

In this chapter we will provide the parton model, the PM, with a QCD field theoretical structure according to the conventional method; for more details see e.g. [52]. In the next chapter we continue the discussion and present the Lund model version of the properties of deep inelastic scattering (DIS) events, both the treatment of the fragmentation and, in particular, the use of the newly developed linked dipole chain model, [16] to provide the fragmenting string state.

The method of virtual quanta (MVQ) in Chapter 2 describes the electromagnetic field from a fast-moving charge in terms of the photon flux from the bremsstrahlung spectrum, and we will make use of this as an analogy. It is evident that Feynman picked up the basic features of the MVQ to make the PM into a description of the corresponding flux of the hadronic field quanta. In that way he made the PM into a useful tool to describe the cross sections for DIS events. Those we consider in this book are initiated by an electromagnetic probe, i.e. they correspond to inelastic electron-baryon (or muon-baryon) scatterings. But it is also possible to use the PM to describe e.g. inelastic neutrino-baryon scattering events as well as to consider the interactions between the partons themselves.

Feynman assumed that the partons can be treated as a stream of free elastic scatterers with respect to the probe. However, at that time there was no known field theory, besides that of non-interacting fields, in which the quanta could even approximately be treated in this way.

All the hadron-hadron cross sections are in the range of tens of millibarns, corresponding to a surface with a radius in the fm region. This is comparable to the size of the hadrons themselves, i.e. their form-factor extensions, cf. section 5.5. In a precise way we may say that within this region the forces are very strong. A hadron is almost black from the point

of view of absorption, which means that (almost) all hadronic probes that penetrate inside the hadronic region are scattered. But we remember from earlier chapters that an electromagnetic cross section behaves as α/Q^2, i.e. it is proportional to the squared wavelength of the probing field and it is consequently small for large Q^2.

We have then two facts which it does not seem possible to explain within the same framework. On the one hand we know that the hadrons interact strongly inside their size radius. On the other hand when they are probed with a wavelength much smaller than this the hadronic wave function can, according to the PM, be projected into a stream of non-interacting partons.

Nevertheless, there is an ingenious answer inside QCD and we will consider it using several different methods. We will discuss in some detail the leading log approximation (LLA) to the relevant Feynman diagrams and we will also consider the lightcone singularities of the current matrix elements we met in Chapter 5. We will show that the two methods are equivalent and can be reformulated into the celebrated DGLAP equations. We will end with a discussion of several suggested corrections.

In section 19.3 there is a brief description of the contents of this chapter to provide the reader with a birds-eye view of the subjects to be covered. But we start in section 19.2 with the general field theoretical method to calculate the cross sections for DIS events. In particular we will clarify the partitioning of the radiation in these states into *initial-state bremsstrahlung* (ISB) and *final-state bremsstrahlung* (FSB). We will make use of these notions repeatedly in this and the next chapter.

19.2   The DIS cross sections, initial- and final-state bremsstrahlung

Until now we have in this book been mostly concerned with the production probabilities in e^+e^- annihilation events. The cross sections for DIS are different and in particular it is not sufficient to know a few low-order perturbative terms in order to describe them. The reason is, of course, the *parton flux factors*, i.e. the hadronic structure functions which we discussed in Chapter 5.

In the MVQ in Chapter 2 the electromagnetic fields of a moving charge are described. These fields, which can be considered as the 'wave functions' of the radiation states connected to the charge, are projected onto states with a fixed frequency ω and impact parameter b (later redefined into the canonically conjugate variable $k_\perp$). Finally the size of the field pulse, or flux, as seen by the measuring setup is described (this corresponds to the squared wave functions). We find that *it only depends upon the number of quanta with quantum numbers* $\omega, k_\perp$.

In Chapter 5 the corresponding flux factors are described as the current-current matrix elements for the probed hadron, cf. e.g. Eqs. (5.49) and (5.66). In this case we sum over all the states which can be reached from the hadron by the application of the current. This result, that there is a close connection between the MVQ radiation wave functions and the current matrix elements, can be inferred from Eq. (5.35). Asking for a particular frequency, sensitive to the probe, means that only the current-current matrix elements which end on this frequency should be included. This corresponds to the Fourier transform of the matrix elements with respect to the probe frequency, in this case given by the momentum transfer q. It is useful to subdivide the radiation into the primary emissions from the currents, called the initial-state bremsstrahlung (ISB), and the remaining radiation, the final-state bremsstrahlung (FSB).

We will, from now on, in general use partonic language and assume that the wave function of the original hadron can be projected onto a set of wave functions with a well-defined number of partons at some observational level. Thus there is, according to the original SLAC experiments, briefly described in Chapter 5, a distribution in x_B, measured at a momentum transfer scale $Q_0^2 \simeq 1$ $(\text{GeV}/c)^2$. This entity is nothing other than the (squared) wave function of the hadron, projected onto the partonic base states. We will now, using this input, construct the (squared) wave function corresponding to a larger resolution scale, as probed by smaller wavelengths $\lambda \simeq 1/Q$. This will be done by an analysis of the Feynman graphs corresponding to multiple gluon emission.

Let us consider, as we shall do more than once later on, the 'fan diagram' in Fig. 19.1. This is not meant as a single Feynman diagram, but rather corresponds to a set of such diagrams. A fan diagram contains a connection, in particular a color flow, from an *incoming parton* (included in the distribution at Q_0^2 and described by a massless energy-momentum vector P) to a *parton scattered by the probe* with energy-momentum q. At this point we will not consider the color connection along the fan diagram.

There is a set of *emissions* along the ladder, described by the energy-momentum vectors p_j (which are always taken to be on-shell and massless). There is also a set of connector lines, to be called *propagators*, described by the energy-momentum vectors q_j, which are all spacelike being the momentum transfers between on-shell lightlike vectors, cf. Chapter 2. At every *vertex* there is energy-momentum conservation,

$$q_j = P - \sum_{m=1}^{j} p_m, \quad \text{i.e.} \quad q_j = q_{j-1} - p_j \tag{19.1}$$

Besides the emitted partons p_j we show a set of further parton emissions, which are (for each index j gathered into a set) called $(h)_j$. We will
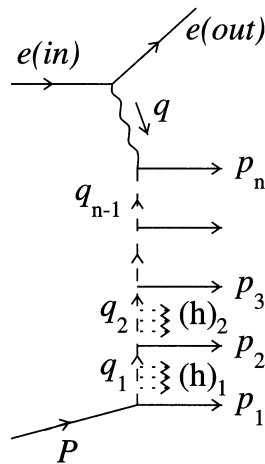
Fig. 19.1. A fan diagram, corresponding to a collection of QCD Feynman graphs between a parton with energy-momentum vector P and a probe with energy-momentum vector q, stemming from the momentum transfer from a leptonic probe e. Notation according to text.

assume that it is possible to emit the set $(h)_j$ according to the rules of a perturbative QCD cascade, i.e. in a coherent way and with negligible recoils, *if we already have emitted the set* (p_j). (Such cascades are the ones we have already encountered in the earlier chapters). The set (p_j) is known as the ISB while the corresponding sets $(h)_j$ are the FSB.

Before we clarify the precise partitioning between ISB and FSB we will exhibit how the cross sections for the radiation states can be described by means of field theoretical Feynman graphs. Consider the configuration in Fig. 19.2, where we again show a set of primary emissions (p_j) along a chain, together with the *radiative corrections* connected to this emission process. Note that we are, as always for the cross sections, considering the square of the production matrix (this time the above-mentioned current matrix) elements, called $\mathscr{J}$ (equal to $\mathscr{J}^*$ because the currents are real), summed over the final-state particles.

While the production matrix elements correspond to the diagrams in Fig. 19.1, the cross sections correspond to the symmetrised graphs in Fig. 19.2 (containing an implicit sum over all the final-state (on-shell) p_j-vectors). It is only the lines along the ladder sides, which are 'true' propagators, carrying the off-shell q_j-vectors. Such diagrams were referred to as *cut diagrams* in Chapter 4 (i.e. cut across the p_j-vectors, which means that the p_j are on the mass shell). Remember that by the renormalisation
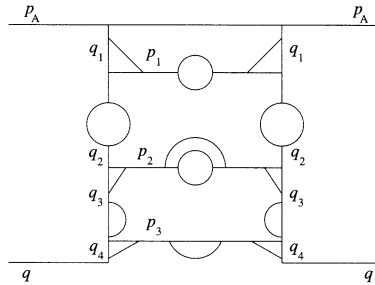
Fig. 19.2. An LLA ladder diagram with a set of radiative corrections along the chain from the incoming parton $P = p_A$ to the momentum transfer q and on the connecting (on-shell) emitted parton lines in between. Note the symmetry between the two sides, a result of summing the matrix elements $\mathscr{J}$ (the left-hand side) multiplied by $\mathscr{J}^* = \mathscr{J}$ (the right-hand side, the same for a real current) over the intermediate states $|X\rangle$ containing the partons p_j.

process the propagators are arranged to have a pole at the mass value of the observed particles, and at the same time a normalisation and a charge value are defined at some (arbitrary) mass scale. The particular diagrammatic contribution in Fig. 19.2 contains such radiative corrections to the normalisation and the charge of the emitted p_j and these contributions can be associated with the sets $(h)_j$, i.e. in the cross section these FSB emissions correspond to radiative corrections, cf. Chapter 4.

We note the close correspondence to the way in which the ladder diagrams occurring in Chapters 9 and 10 describe the states that can be reached by the hadronic scattering operator T (and from the other side by $T^\star$). We may take over from these discussions the fact that in order to obtain a large contribution from such diagrams the momentum flowing along the lines should not be (too) large. Therefore, if the external probe's energy-momentum $q^2 = -Q^2$ increases then it is necessary to include more and more rungs in the ladder diagram.

The problem is to distinguish the two sets, i.e. those gluon emissions that are included in the set (p_j), and those in the sets $(h)_j$. Actually there is no clear distinction apart from the two features mentioned above, that in order to be able to 'sum away' the set $(h)_j$ as virtual corrections to the main p_j-emissions they should be coherent and leave small recoils. We are not allowed to make statements about time-ordering, as we found in Chapter 16 in connection with Figs. 16.1 and 16.2. None of the contributions from the single graphs is gauge-invariant by itself and although it may seem natural to partition them into a 'before' and 'after' scenario such a partitioning is not consistent.

The answer is that any choice of the q_j-emissions is allowed. But a particular choice will also contain a corresponding set of virtual corrections of the Sudakov kind, i.e. there will be a Sudakov factor for each choice, in accordance with the discussion in section 17.3. The cross sections of DIS are then given by the formula

$$d\sigma_{DIS} = \sum_I dw(I)Sud(I) \qquad (19.2)$$

where $dw(I)$ is the inclusive weight for emission of a state I, i.e. an inelastic state included in the initial-state bremsstrahlung. If we change the content of the set of I-states this will be compensated by a corresponding change in the Sudakov factor $Sud(I)$ so that the sum is unchanged. At this point it is worthwhile to be a little more specific because the cross section is an observable quantity. It would be rather puzzling if a particular state provide different contributions solely because of our ISB choice.

Consider an exclusive partonic state in a DIS event, i.e. consider all the gluonic radiation emitted in a state. Then we may subdivide this radiation into the ISB part, defined by some rule or another, and the rest, the FSB. The total weight for the state is then given by the weight for the ISB choice, denoted $dw(I)Sud(I)$ in Eq. (19.2), *together with a Sudakov factor* $dw(F)Sud(F)$, *corresponding to the probability of emission the particular FSB group(s) from the chosen ISB state.* Remembering the properties of the Sudakov factors, cf. section 17.3, *we conclude that $dw(I)Sud(I)$ corresponds to the contribution from the sum over all states with the same ISB choice and all possible FSB gluons resulting from them.* If we change the ISB set then the weight for the exclusive state must be rearranged:

$$dw(I)Sud(I)dw(F)Sud(F) \rightarrow dw'(I)Sud'(I)dw'(F)Sud'(F) \qquad (19.3)$$

and we obtain the primed ISB contribution to the cross section after summing over all the states defined by the new ISB gluons and all allowed (primed) FSB in these states. But the total result in Eq. (19.2) is the same!

19.3 A bird's-eye view of the features of deep inelastic scattering

1 Generalities on the leading-log approximation

There were, rather soon after the PM was suggested and the original SLAC experiments were completed, serious attempts by Gribov and his collaborators to provide a consistent method of re-summing the higher-order terms in perturbation theory. For DIS events they arrived, with due care to the Sudakov corrections discussed above, cf. [52], at the results which are known as the leading-log approximation (LLA), valid for field theories with a dimensionless coupling constant.

They found that in every order of perturbation theory there are new (in general squared) logarithmic contributions in the large variables such as the squared cms energy s. The sum of such contributions tends to grow exponentially so that the logarithms become powers in s. (The reason that there are two logarithmic powers is that both the transverse momentum and the rapidity variations provide contributions, although both of them will at the nth order be limited due to the iterations by inverse factors of $n!$, cf. Eq. (19.6) below.)

In DIS, where there are two basic dynamical variables Q^2 and v, there are problems when these variables are not of the same order, i.e. when x_B is very small. Then it is necessary to sample the double logarithms in Q^2 and $1/x_B$, but the power correction results are still true. This means a serious disagreement with the scaling results from SLAC and in particular that the PM could not be motivated within such a framework.

A major advancement at the theoretical level started when it was recognised, [68], that nonabelian gauge theories exhibit *asymptotic freedom*. The coupling constant for these theories does not behave as in other theories; cf. Chapter 4. Instead *the nonabelian coupling constants effectively become smaller when the momentum transfers increase*.

This is partly sufficient, although not enough, to obtain the original scaling arguments of the PM. A typical result might be if one calculates the multiplicity from the contributions of the ladder diagrams,

$$\sum_n \frac{[C\alpha_s \log^2(s/s_0)]^n}{(n!)^2} \tag{19.4}$$

In order to understand the behaviour of this sum we make use of the Stirling approximation for large values of n,

$$n! \simeq \exp[(n+1/2)\log(n+1) - (n+1)] \tag{19.5}$$

and maximise the expression with respect to n. For positive values of d a sum of the following kind

$$\sum \frac{a^{dn}}{(n!)^d} \simeq \exp(ad) \tag{19.6}$$

is strongly governed by the term corresponding to this maximum, i.e. by the term with $n_{max} \simeq a$. Therefore the sum in Eq. (19.4) will behave like a power in s for a constant coupling α_s. But if the coupling behaves, as in QCD, effectively like $1/\log s$, the result in Eq. (19.4) will behave, as in our calculations of λ and the multiplicities in Chapter 18, like $\exp(c\sqrt{\log s})$. There will be scale-breaking logarithmic behaviour but there will not be power corrections within this framework.

We have also seen that, in accordance with the Callan-Symanzik equations in Chapter 4, there will be logarithmic power corrections to some

quantities. This is a reflection of the same feature, i.e. that *asymptotically free theories involve some scale-breaking 'on the way to freedom'*.

Thus even inside QCD the partonic flux factors will contain a Q^2-dependence so that we should write, for the parton distributions in Chapter 5, $f(x_B, Q^2)$. In this and the next chapter we will consider this Q^2-dependence, which actually occurs as a dependence on

$$\tau = \log(Q^2/\Lambda_{QCD}^2) \tag{19.7}$$

We will investigate it from several different points of view but we note that such logarithmic corrections generally are slowly changing when $Q \gg \Lambda$.

2   *Generalities on the moment method and the operator product expansion*

We have already in Chapter 5, subsection 1, presented the reasons to go to a lightcone dynamical treatment of the matrix elements which occur in DIS. The structure functions f are given by the Fourier transforms of the squared current matrix elements but this result can be reformulated in terms of commutator matrix elements, which should vanish (according to causality) outside the lightcone. Therefore we found that the structure functions should in limiting situations be dominated by the current behaviour along the lightcones.

After a brief discussion of the kinematics we will use this lightcone dynamical treatment in terms of the moment method (MM) combined with the Wilson lightcone operator product expansion (OPE) in a way invented by Christ, Hasslacher and Mueller, [43]. (The historical and intellectual dependence of the results is outside the scope of this book. It is, however, evident that the original participants in the LLA adventure very early noted the simplicity of their results in terms of the moments of the structure functions.)

This treatment will lead to a description of QCD scale-breaking, [69], for the moments of the structure function f:

$$\mathscr{F}(j, Q^2) = \int_0^1 x^j dx f(x, Q^2) \sim \mathscr{F}(j, Q_0^2) \left(\frac{\alpha_s(Q_0^2)}{\alpha_s(Q^2)} \right)^{a_j} \tag{19.8}$$

Here Q_0^2 is a fixed scale (introduced above), $\alpha_s(Q^2)$ is the running coupling of QCD and the a_j are numbers that can be computed by means of the MM and the OPE.

We will present the physical arguments within a scalar field theoretical framework. The situation for the real world is somewhat more complex because there are vector indices as well as dimensional differences in connection with electromagnetic currents. There are also several flavor- and color-dependent contributions to the different parts of the parton distributions but the result in Eq. (19.8) is true for each part.

The MM, combined with the OPE, corresponds to a very neat method. It relates the moments of the structure functions to the behaviour of the matrix elements of space-time operators. Then the renormalisation group, in terms of the Callan-Symanzik equations [108] (cf. Chapter 5), is applied to the operator matrix elements to obtain the results in Eq. (19.8).

The method turns out to be equivalent to the LLA. If we invert the results for the moments in Eq. (19.8) we obtain a set of integro-differential equations, nowadays known as the DGLAP equations, for the structure functions $f(x_B, Q^2)$ (DGLAP is short for Dokshitzer-Gribov-Lipatov-Altarelli-Parisi). These equations are equivalent to the results derived within the LLA, [52], which means that the whole setup is consistently connected. It turns out that the Sudakov factors in this case simply correspond to a subtraction in the occurring splitting functions to fulfil the energy-momentum conservation constraints.

In this way a 'conventional' scenario emerges, which will be called the *ISB scenario*. Viewed from the lightcone point of view, larger values of Q^2 will probe regions closer and closer to the lightcone, cf. Chapter 5. Remembering that the variable x_B is the Fourier inverse of the variable px, we conclude that small values of j in Eq. (19.8) correspond to probing large distances along the lightcone direction px and large values of j correspond to probing small regions close to the origin.

For small values of j the numbers a_j in Eq. (19.8) are generally positive, meaning that the small-x_B region will increase in the structure functions. The a_j's turn round and become negative for larger values of j; then the main contributions to the moment integrals come from the large-x_B part of the distributions. Viewed from the LLA perspective, an increase in Q^2 corresponds to the possibility that a parton at Q_0^2 may split up into smaller-x_B partons at a higher scale of resolution. This is of course the same dynamics as before, namely that the small-x_B region obtains more and more contributions, as Q^2 increases, from the partons which decay along the fan diagrams, thereby depopulating the larger x_B-values.

3   *Some problems in the ISB scenario*

There are nevertheless a set of problems. Some of these are addressed in the work by Gribov jr, Levin and Ruskin (GLR) [67]. They are related to the uncomfortably large numbers of partons which may emerge at small-x_B and moderate-to-large Q^2 values from the ISB scenario.

GLR re-sum a set of Feynman graph contributions to calculate the probability that some of the already emitted partonic 'chains' reinteract, thereby decreasing the total partonic multiplicity, cf. also [95]. But this so-called *shadowing* method (where one emitted chain is in front of another

emission) is only applicable inside certain regions of phase space and outside these there are more complex multiparton interactions.

The correction terms contain an unknown scale corresponding to the (transverse) region effectively inside which a parton chain is emitted. If this scale is determined by the expected hadronic size, around 1 fm, then the correction terms are rather small and the multiplicity growth of the partons at small x_B is not inhibited at the presently available energies.

It is, however, possible to imagine that the hadronic wave functions contain large- and small-density regions in a complex way, so that there are 'hotspots' of a small size, which will then provide large GLR corrections.

There are also other reasons for concern about the ISB scenario. To begin with, the MM and OPE results coincide with the LLA because both of them pick out only the leading contributions and neglect all corrections. Thus in the MM and OPE all non-scaling contributions are neglected and only the leading singularities on the lightcone, corrected by the logarithms from the renormalisation group equations, are retained. For the LLA, to all orders only the terms with the largest logarithmic factor are retained (it is, however, possible to use a modified leading-log scenario such as described in Chapter 18).

There have been efforts by Lipatov and his coworkers, [29] to take account also of (some of) the non-leading contributions. The result of their effort is, however, that the number of small-x partons increases even more, although it then tends to stabilise for the evolution equations.

The Lipatov results are that e.g. the gluon structure function will, for small x behave like a power in x (there is also some gaussian $\log Q^2$-behaviour, due to the projection on an eigenfunction):

$$g(x) \sim x^{-1-\lambda_L} \tag{19.9}$$

where λ_L is a number of order 0.5, stemming from the largest eigenvalue of an integral equation.

These results should be valid for medium to small Q^2. They imply that the ocean $q\bar{q}$-content of the nucleon structure functions, which is directly coupled to the gluon density, will make the cross sections very large indeed for increasing energies (which means that unitarity must be invoked and/or shadowing à la GLR). We will call this effect the *BFKL mechanism* (for Balitsky-Fadin-Kuraev-Lipatov). We will also point out that there are large corrections to the results in Eq. (19.9) both from energy-momentum conservation and from the QCD coherence conditions.

Note that the coherence conditions of QCD bremsstrahlung are not necessarily applied within the DGLAP and BFKL approaches. In section 19.6 we will consider the approach of Marchesini *et al.*, [44], in order to show the implications of a more sophisticated approach, which contains both the DGLAP and the BFKL contributions but nevertheless retains

the coherence conditions. This is also the starting point of the linked dipole chain model, [16] to be described in the next chapter.

19.4 The moment method and the DGLAP mechanism

1 Kinematical preliminaries

There are several coordinate systems of interest used for the description of DIS events. One is called the *probe-hadron cms*. We will in this chapter mostly make use of this system or rather of a system which is somewhat more general, called 'equivalent to the hadron-probe cms'. This means that we boost along the momentum direction (conventionally the 3-axis) between the probe and the hadron. Then the probe q will have light-cone energy-momentum components ($\mathbf{0}_\perp$ stands for vanishing transverse momentum)

$$q = (-Q_+, \mathbf{0}_\perp, Q_-) \tag{19.10}$$

The hadron is in this frame described by a (large) lightcone energy-momentum $P_+ = E + P_3$. We neglect its transverse (i.e. along the (1,2)-axes) and negative lightcone components. We will assume that the hadron is described by P_+ and by its space-time component $x_{+3} = t + x_3$. This is compatible with quantum mechanical considerations since the quantities P_+ and x_{+3} commute. Thus the hadron is described by a wave function depending upon P_+, x_{+3}.

We may then consider the interaction as a *measuring process* in which the probe determines the hadron's x_{+3}-coordinate to a precision given by the 'interaction time', $\delta x_{+3} \simeq 1/Q_-$. The hadronic state can then be in any of its eigenstates within the energy-momentum range (P_+, P_-) with $P_- \leq Q_-$. These are the quantum states which live sufficiently long (at least as long as the interaction time) for a measurement to take place.

The measuring process is defined by an interaction with a parton with $x_B P_+ = Q_+$; the parton is then turned around by the momentum transfer so that the final state corresponds to a hadronic state in the energy-momentum range $(P_+ - Q_+ \equiv P_+(1-x_B),\ Q_-)$. The phase space for gluon emission is evidently described by the triangular region in Fig. 19.3 in terms of the parton variables $\kappa = \log(k_\perp^2/s_0)$ and rapidity y.

The various useful kinematical variables are exhibited in Fig. 19.3. We note that a fixed value of the fractional energy-momentum $x = k_+/P_+$, with $k_+ = k_\perp \exp y$, corresponds to a straight line across the triangle. In particular, for $x = x_B$ we obtain a triangle corresponding to Q^2 on the left-hand side of the total phase-space triangle. We also note that the length of the baseline of the triangle corresponds to $\log W^2 = \log(P_+ Q_- - Q^2) \simeq \log P_+ Q_-$ (the approximation is valid unless $x_B \sim 1$). All partonic emission,
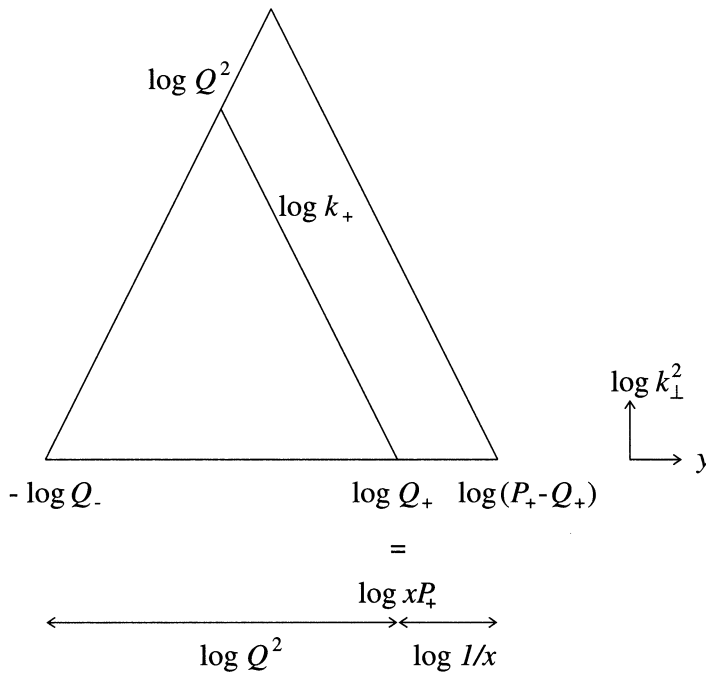
Fig. 19.3.   The phase space for emission of gluons in a DIS event.

whether it should be referred to as ISB or FSB radiation, must occur inside this triangle in an energy-momentum conserving theory.

There are various intuitive pictures that can be used to imagine the hadronic state. In the ISB scenario it is useful to think of a virtual excitation living for a long time due to time dilation (cf. Chapter 2). Such an excitation may then be described as a cascade chain, which in a coherent way develops and then reassembles.

In this way there may be many chains available, each starting on a 'permanent' member of the wave function. The interaction probe will pick out one parton with fractional energy-momentum x_B, thereby breaking the coherence in that particular chain and realising the corresponding radiation state, see Fig. 19.4. This diagram is taken from [67] where a particularly lucid description is given of the ideology behind the ISB scenario.

2   *The moment method based upon Wilson's operator product expansion*

This section contains many formal notions and, although the mathematics will be rather informal, this is a worthwhile approach since we can then
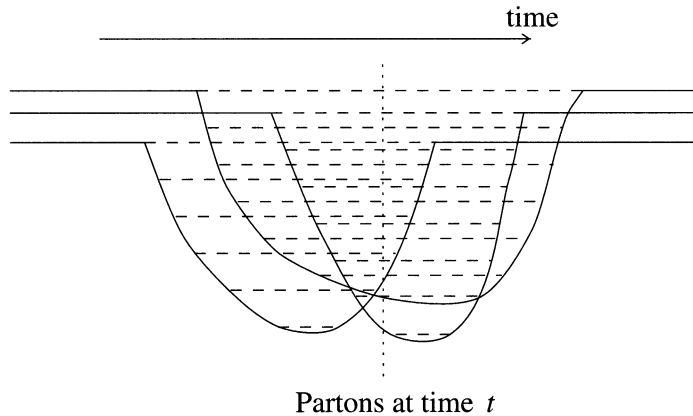
time

Partons at time t

Fig. 19.4. A possible set of radiation chains (shown by broken lines) starting, evolving and reassembling. The probe (not shown) will interact with one parton in a chain and break the coherence in that particular chain.

present some basic physical ideas as well as some useful analysis methods. The reader not interested in the details may go directly to Eq. (19.20), which in an intuitive way describes the developments that go before.

We would like to isolate the major contributions to the current matrix element in Eq. (5.49), which describes the cross section in DIS reactions. This is done by an expansion around the lightcone singularities of the current commutator. A field operator is distribution-valued but we may nevertheless (with care) use a pointlike notation both for the free-field operators and also for the perturbed-field operators in an interacting theory, [36], although in that case after renormalisation.

The relationship between the time-ordered and normal-ordered operator products, which was derived in Chapter 3, implies for the current $j(x) = \lim_{y \to x} :\Phi(x)\Phi(y):$:

$$
\begin{aligned}
j(x)j(0) \overset{x_\mu \to 0}{\to} \ & c_0 \frac{1}{(x^2)^2} I + c_1 \frac{1}{x^2} j(0) \\
& + c_2 \frac{1}{x^2} x_\mu :\Phi \partial^\mu \Phi:(0) + c_3 :jj:(0)
\end{aligned}
\tag{19.11}
$$

The numbers c_j are constants for free fields and I stands for the unit operator. This is the original *Wilson short-distance expansion of an operator product*, in which one only takes the singular terms into account. As mentioned above, [36], it is well defined also in perturbation theory but then the numbers c_j become logarithmic functions of x.

We would now like to go over to the lightcone scenario described in

Chapter 5. We note that for a short-distance expansion such as Eq. (19.11), when each component of the vector x_μ tends to zero, then $1/x^2$ is one power more singular than x_μ/x^2. But when we consider the approach to the lightcone, $x^2 \to 0$, then these expressions are both equally singular. In this limit it turns out that one needs an infinite number of local-operator terms:

$$j(x)j(0) \overset{LC}{\to} c_0 \frac{1}{(x^2)^2} I + \frac{1}{x^2} \sum_{m=0}^{\infty} f_m x_{\mu_1} \cdots x_{\mu_m} O^m_{\mu_1,\ldots,\mu_m}(0) + \cdots \quad (19.12)$$

The limit notation LC means the lightcone limit $x^2 \to 0$. The operators O^m are all the (local and symmetric) operators in the field theory that carry m Lorentz indices (we use the summation convention for repeated indices μ_j). As an example, in a theory with a scalar field Φ there will be, for the corresponding currents, an $O^m_{\mu_1,\ldots,\mu_m} = \, : \Phi \bar{\partial}^{\mu_1} \cdots \bar{\partial}^{\mu_m} \Phi : (0)$ where the notation $\Phi \bar{\partial}^\mu \Phi = \Phi (\partial/\partial x^\mu)\Phi - [(\partial/\partial x^\mu)\Phi]\Phi$ has been used repeatedly.

It is obvious that along the lightcone all the quantities in the sum have the same singularity, i.e. $1/x^2$. The final ellipses refer to less singular terms in the expansion. The idea behind the partitioning in Eq. (19.12) is *to find for each field theory the basic operators O^m, express them in terms of the free-field correspondences and then to include all the perturbation theoretical modifications in the coefficients f_m.* From perturbation theory with non-dimensional coupling it is possible to prove, [36], that the f_m are functions of $\log x^2$ expressible as power series in the coupling g:

$$f_m(x^2) = \sum_{j=0}^{\infty} \sum_{r=0}^{r=j+1} f_m(j,r) g^{2j} \log^r x^2 \quad (19.13)$$

From the results in Eqs. (19.12) and (19.13) we have a method of analysing the current matrix elements in Eq. (5.49). We firstly note that if we evaluate the tensor O^m in a state with a well-defined energy-momentum p we will, due to Lorentz covariance, obtain

$$\langle p| O^m_{\mu_1,\ldots,\mu_m} |p\rangle = p^{\mu 1} \cdots p^{\mu m} C_m + \cdots \quad (19.14)$$

The reason is that p is the only Lorentz vector available in a scalar theory. The so-called 'reduced matrix element' C_m is, in a free-field theory, a plain number and in this way we have been able to extract the 'trivial' Lorentz covariance requirement.

If we consider the Fourier transform of the current matrix element itself we obtain from Eqs. (19.12) and (19.14)

$$\mathscr{W} \equiv \int dx \exp(iqx) \langle p|j(x)j(0)|p\rangle$$

$$= \int dx \exp(iqx) \sum_m f_m(x^2)[(px)^m C_m + \cdots] \frac{1}{x^2 + i\epsilon x_0} \quad (19.15)$$

The power $(px)^m$ is, using the notation $(P_+, \simeq 0, \mathbf{0})$ for p, given by the expression $[(P_+ x_-)/2]^m$ and can, at least formally, be written as

$$(px)^m \exp(iqx) = (i2pq)^m \left(\frac{\partial}{Q_- \partial Q_+} \right)^m \exp(iqx) \tag{19.16}$$

This means that the whole expression can be rewritten as

$$\mathcal{W} = \sum_m \frac{1}{x_B^{m+1}} C_m E_m,$$

$$iv E_m = (iQ^2)^{m+1} \left(\frac{\partial}{\partial Q^2} \right)^m \int dx \exp(iqx) f_m(x^2) \frac{1}{x^2 + i\epsilon x_0} \tag{19.17}$$

In this derivation we have freely interchanged sums and integrals and performed a set of formal operations such as the differentiations in Eq. (19.16). What we have obtained is an approximate expression for the quantity $\mathcal{W}$ in terms of a power series in (the inverse of) x_B multiplied by the matrix element functions C_m and the c-number functions E_m. In this way we have been able to rewrite the power series in px, in Eq. (19.15), as an inverse power series in x_B, which once again reminds us of the reciprocal relationship between these variables.

In order to relate the quantities C_m and E_m to measurables, it is necessary to make an assumption on analyticity for the quantity $\mathcal{W}$ in respect of the variables x_B and Q^2. In [43] the authors assume that $\mathcal{W}$ is, *for large values of Q^2, an analytic function of x_B apart from branch cuts for $-1 \le x_B \le 1$.* It is not possible to prove this statement outside perturbation theory so we are thus in the same situation as for the elastic form factors in Eq. (5.47).

The authors of [43] also assume that $\mathcal{W}$ is even in x_B (which corresponds to the property of crossing, in a field theory). Therefore we can use Cauchy's formula for the line integral around a curve c of an analytic function to write the function $x_B^n \mathcal{W}$ as follows:

$$\frac{1}{2i\pi} \oint_c dx_B x_B^n \mathcal{W} = C_n E_n \tag{19.18}$$

$$= \frac{1}{2i\pi} \int_0^1 dx_B x_B^n [\mathcal{W}(x_B + i\epsilon) - \mathcal{W}(x_B - i\epsilon)] \tag{19.19}$$

Now the integrand on the right-hand side is $2i \, \text{Im}(\mathcal{W})$ and can be identified with the physically measurable quantity $W = 2\pi \tilde{f}(x_B, Q^2)/v$ discussed in Chapter 5. In Eq. (19.18) we have used the residue calculus and have diminished the Cauchy curve to include only an integral along the singularities lying on the cuts, using the symmetry $\mathcal{W}(-x_B) = \mathcal{W}(x_B)$ mentioned above.

Consequently, the nth moment of the structure function $\tilde{f}$ in this scalar theory can be identified with the (reduced) matrix element C_n multiplied

by the c-number function E_n. This in turn can, according to Eq. (19.17), be expressed as the Q^2-variation of the (energy-momentum space) matrix element of the operator O^m, evaluated in perturbation theory. This should remind us of the Callan-Symanzik equation, discussed in Chapter 4, which describes just this, i.e. the effect on a matrix element stemming from scale changes in the renormalisation. Therefore if we perform the renormalisation just at the point Q^2 (which is allowed according to the assumptions on analyticity) we may apply the Callan-Symanzik formalism to derive the behaviour of the moments of the structure function!

We can thus summarise our results in the following simple statement (although it contains some subtle relations)

$$\int_0^1 dx_B x_B^m \tilde{f}(x_B, Q^2) \propto \frac{1}{(P_+)^m} \langle p | O_{++\cdots+}^m | p \rangle_{Q^2} \qquad (19.20)$$

The matrix element on the right-hand side is then evaluated in energy-momentum space and renormalised at the scale Q^2 according to Chapter 4, [52]. Within perturbation theory, it will coincide with the product $C_m E_m$ obtained in Eq. (19.18). It is, however, necessary to understand that there are at least two important aspects of this result. Firstly there is the assumption that the approximation of keeping only the most singular terms from perturbation theory in the lightcone expansion is a good one. Secondly it is necessary to invoke analyticity for the function $\mathscr{W}$ in order to derive the relationship of the moments to the derivatives of the matrix element.

3 The Callan-Symanzik equation and its implications for the moments

We will now use the *renormalisation group* of field theory, Chapter 4, to calculate the behaviour of the quantities E_m in Eq. (19.17) when Q^2 varies. The tool will be the Callan-Symanzik equation and we will extend it outside the scalar field theory scenario we have considered up to now.

We recall that the β-function of QCD is negative,

$$\beta(\alpha) = -b\alpha^2 - \cdots \qquad (19.21)$$

where the ellipses refer to higher-order terms, some of which have been calculated; but they do not play a major role in our argument. This implies that the QCD running coupling vanishes as the inverse of the log of the scale at which we perform our renormalisation. We may choose this scale at Q^2 (it is allowed according to the analyticity assumptions in the MM and OPE) and consider the large-Q^2 limit just as in the treatment of the Callan-Symanzik equation in Chapter 4. Because of the properties of the running coupling we need only the lowest-order perturbation theory results to calculate the anomalous-dimension functions γ.

In [69] the anomalous dimensions of the operator matrix elements $C_m E_m$ are calculated for QCD. They are unfortunately not as simple as the ones we encountered in Chapter 4, where $\gamma_m = d_m \alpha_s$, the d_m being plain numbers and α_s the QCD coupling. There are two reasons. The first is the tensor structure and the dimensions of the electromagnetic currents, but those cause only minor complications in comparison with the scalar version of the MM discussed in the last subsection.

The major reason for the complications is that in this case there are contributions to the current matrix elements not only from quark and antiquark intermediate states but also from the gluon states that can be reached by applying the gluon field operator A. This means that both of the matrix elements

$$\langle q | AA | q \rangle, \quad \langle q | j | q \rangle \tag{19.22}$$

are nonvanishing; thus a quark can be absorbed not only by the fermion current j but also by the gluon 'current' AA stemming from the three-gluon interaction of QCD. In Eq. (19.22) we have neglected all vector and color indices.

The fact that both the matrix elements are nonvanishing can be understood from our considerations relating the scattering from a potential to the scattering from protons in Chapter 5, cf. Eq. (5.35). There we used that

$$A^\mu(x) \to \int dx_1 \Delta_F(x - x_1) j_B^\mu(x_1) \tag{19.23}$$

This means that the matrix elements of the potential A behave like the corresponding (color) current ones *and they are nonvanishing*. Therefore the OPE couples any current to both the quark and the gluon contributions. This feature is called *operator mixing*. Then we obtain a *matrix form of the Callan-Symanzik equation* in this case, written for a matrix $E(m)$ instead of the plain function $E(m)$, in Eq. (19.17):

$$E(m) = \begin{pmatrix} E_{NS}(m) \\ E_q(m) \\ E_g(m) \end{pmatrix} \tag{19.24}$$

The indices refer to non-singlet, i.e. the valence flavor parts, cf. Chapter 5, and to quark (q) and gluon (g), respectively, and we get

$$\left[\mu \frac{\partial}{\partial \mu} + \beta \frac{\partial}{\partial \alpha} - \gamma(m) \right] E(m) = 0 \tag{19.25}$$

Here the β-contribution is diagonal and m-independent, $\beta = -b\alpha^2$, but

$\gamma(m)$ is non-diagonal with the numbers $d = d(m)$ plain numbers:

$$\gamma = \alpha \begin{pmatrix} d_q & 0 & 0 \\ 0 & d_q & 2n_f d_{qg} \\ 0 & d_{gq} & d_g \end{pmatrix} \qquad (19.26)$$

This is a linear equation and, like any linear equation, can be diagonalised by taking combinations of the quark and the gluon components to obtain 'eigenstates' and in particular 'eigenfrequences' from the diagonalised γ-matrix elements. We will not do this, nor will give the formulas for the numbers d, because it is done in detail in the original papers, [69], as well as in [52].

The main point is that the different elements of the matrix E in Eq. (19.24) can be written as linear combinations of the following kind:

$$E_j(m) = \sum_i (\xi)^{\delta_{ji}(m)} \mathscr{E}_i(m), \quad \xi = \frac{\alpha_1}{\alpha_s(Q^2)} \qquad (19.27)$$

(this means that the E_j behave as powers in $\log Q^2$!). The powers δ are derivable from the matrix elements in Eq. (19.26) and the coefficient in the QCD runnning coupling and the quantities $\mathscr{E}_i(m)$ are the initial values of the moments at the scale where the running coupling is α_1. Thus *the moments of the structure functions for both quarks and gluons will, according to this result, contain computable logarithmic power corrections in the large-Q^2 limit.* This behaviour is very well confirmed experimentally, at least inside the presently available Q^2-region.

For the non-singlet moments, in particular, there is only one term in the sum and it corresponds for each moment m to $\delta_m = d_q^{(m)}/b$. Therefore we have in this case the simple differential equation

$$\frac{dE_{NS}^{(m)}}{d\tau} = d_q^{(m)} \alpha_s E_{NS}^{(m)} \qquad (19.28)$$

where τ is defined in Eq. (19.7). The general results can be reformulated into a relation between τ-derivatives of the matrix E and the γ-matrix:

$$\frac{dE(m)}{d\tau} = \alpha_s \gamma(m) E(m) \qquad (19.29)$$

4   The DGLAP equations

As we have said before this is not the place to discuss the historical and intellectual developments with respect to 'who did what first'. But it is evident that many different contributions did occur independently.

One major contribution to the understanding of the physics is given in [5], where it is proved that the differential equations for the moments in Eq. (19.29) can be rearranged into equations for the parton structure functions

themselves, nowadays known as the DGLAP (Dokshitzer-Gribov-Lipatov-Altarelli-Parisi) equations:

$$\frac{dq_j}{d\tau} = \alpha_s \int_x^1 \frac{dz}{z} \left[\mathscr{P}_q^q(z) q_j \left(\frac{x}{z}, \tau \right) + \mathscr{P}_{q_j}^g(z) g \left(\frac{x}{z}, \tau \right) \right] \tag{19.30}$$

$$\frac{dg}{d\tau} = \alpha_s \int_x^1 \frac{dz}{z} \left[\sum_j^{2n_f} \mathscr{P}_g^{q_j}(z) q_j \left(\frac{x}{z}, \tau \right) + \mathscr{P}_g^g(z) g \left(\frac{x}{z}, \tau \right) \right]$$

The index j corresponds in this case to different q- and $\bar{q}$-flavors and we obtain back the splitting functions which were derived in Chapter 17, $\mathscr{P}_b^a$, for the splitting of a parton a into a parton b (cf. below for the behaviour of $\mathscr{P}$ when its argument approaches unity).

The main part of the proof in [5] is to show that the anomalous dimension matrix $\gamma(m)$ fulfils the identity

$$\gamma(m) = \begin{pmatrix} d_q(m) & 2n_f d_{qg}(m) \\ d_{gq}(m) & d_g(m) \end{pmatrix} = \int_0^1 dz\, z^m \begin{pmatrix} \mathscr{P}_q^q(z) & 2n_f \mathscr{P}_g^q(z) \\ \mathscr{P}_q^g(z) & \mathscr{P}_g^g(z) \end{pmatrix} \tag{19.31}$$

This is straightforward if we use the formulas for the splitting functions and for the anomalous-dimension matrix. After that one can rely on a mathematical theorem which tells us that a moment equation can be inverted in a unique way. (The observant reader may note that the first equation of (19.30) has been summed over the different q-flavors.)

The even more observant reader will note that some of the splitting functions are singular for $z = 1$ and therefore the integrals in Eqs. (19.30) and (19.31) are not well defined. A closer examination tells us, however, that this singularity is closely related to energy-momentum conservation. Formally it turns out that the singular behaviour of the splitting functions (this is shown in detail in [52]) is cancelled by a proper account of the virtual corrections to the emissions.

The result for the non-singlet is obtained by taking the difference between the equations for the derivatives of two quark (or antiquark) species. In that way the gluon term in the first equation of (19.30) vanishes and we obtain a diagonal contribution from the same difference between the structure functions integrated over the $q \to qq$ splitting function.

There is a direct connection between the results using the MM and the OPE, as in [43] and [69], and the LLA results of Gribov and collaborators, [52]. For the latter case one follows the emission lines in high-order perturbation theory and rewrites the results as exactly the integro-differential equations (19.30).

In order to understand the physics we consider again the phase-space triangle; see Fig. 19.5. Suppose that we increase Q^2 for a fixed value of P_+, i.e. of the hadron energy, and for a fixed value of $x = x_B = Q_+/P_+$. This means that the left-hand side of the triangle, $-\log(Q_-)$, will move to
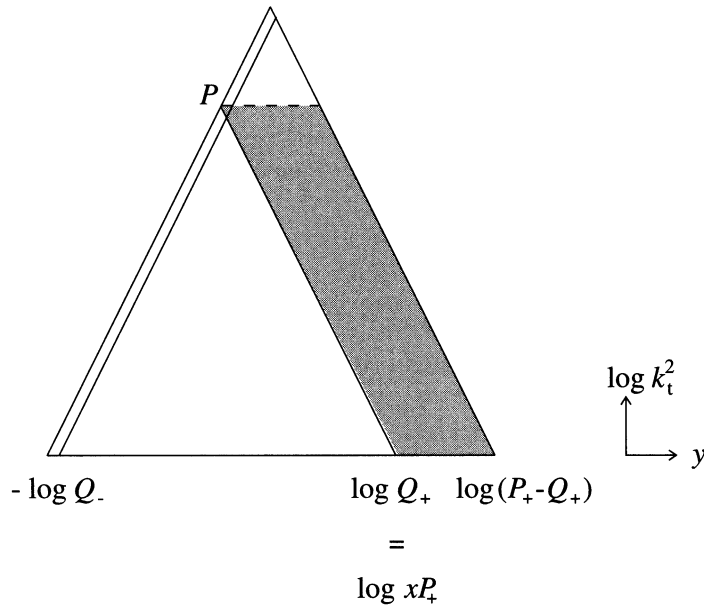
Fig. 19.5. The phase space corresponding to the emission of new partons at x, following an increase in Q^2, is shown, together with the region (shaded) inside which one must in an ISB model know which partons already exist.

the left. Then the DGLAP equations (19.30) describe the change of the structure function at the point P, corresponding to $k_\perp^2 = Q^2$ and x. This is the left-hand side of Eq. (19.30). On the right-hand side the change is related to the number of partons with values $x' > x$, each of which, due to the QCD processes that are possible, may decay into a parton at x. The region inside which we may sample such partons is shaded in Fig. 19.5.

Suppose that we consider such a parton decay, Fig. 19.6. The incoming parton will have a fraction x' of the hadron P_+, and we will assume for simplicity that it is massless. It will emit a massless gluon with $x_g = (1-z)x'$ thereby becoming a virtual parton with lightcone fraction $x = zx'$. Its virtual squared mass, which is usually related to the value $-Q^2$, can be calculated from the transverse momentum, $k_\perp$, in the emission by

$$Q^2 = \frac{k_\perp^2}{1 - z} \tag{19.32}$$

The transverse momentum variable, $k_\perp$, is compensated between the two partons emitted, so that they have $\pm \mathbf{k}_\perp$ respectively, and the result of Eq. (19.32) stems from the conservation of the negative lightcone component.

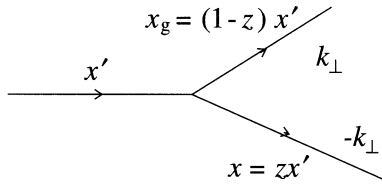The probability for the emission shown in Fig. 19.6 is given by the

Fig. 19.6.   The kinematics of parton decay with notation as discussed in the text.

splitting function, $\mathscr{P}(z)$, multiplied by the density of such partons, i.e. the relevant structure function at $x' = x/z$, and by the coupling. The result must be summed over all possible partons and integrated over all values of x', giving the right-hand side of Eq. (19.30).

5   More on the leading-log approximation

In Chapter 5 we derived the hadronic tensor $W_{\mu\nu}$, Eq. (5.49). In Fig. 19.2 we have shown a contribution with intermediate state $|X\rangle = |p_1,\ldots,p_n\rangle$; here $n = 4$. The state is produced by iteration (including the radiative corrections) along a main chain with propagators redistributing the large momentum transfer q into many rungs of the ladder. Although there are obvious similarities to the ladder diagrams for the unitarity equations in Chapter 10, the kinematics is different in this case, in which the virtuality is building up and the energy-momentum fraction is decreasing down the main chain.

   The result in the LLA is that the main contributions stem from diagrams having the kinematical variables of the q_j-emissions *strongly ordered*:

$$q_{\perp 1} < q_{\perp 2} < \cdots < q_{\perp n} < Q; \quad 1 > z_1 > z_1 z_2 \cdots > x_B \equiv \prod z_j \quad (19.33)$$

The motivation is that to avoid strong damping from the propagators the large momentum transfer Q^2 must be partitioned over many steps. The larger is Q^2, the more steps are necessary for the energy-momentum flows in each rung of the diagram to be reasonably small.

   If we use the approximate weight dw_j for every step (putting the gluon splitting function $\mathscr{P} \sim 1/z$ and $\log q_\perp^2 = \kappa$),

$$dw_j \sim \bar{\alpha}(\kappa) d\kappa_j \frac{dz_j}{z_j} \quad (19.34)$$

then, using the ordering given in Eq. (19.33) and the symmetrical re-

summation we have used before,

$$\int \prod_{j=1}^{n+1} dy_j \Theta(y_{j-1} - y_j) = \frac{Y^n}{(n)!}, \quad \chi(Q^2) = \int_{\log Q_0^2}^{\log Q^2} \frac{\alpha_0}{\kappa} d\kappa \qquad (19.35)$$

we obtain the sum of the main contributions:

$$xg(x, Q^2) \sim \sum_n \frac{[\chi(Q^2) \log(1/x_B)]^n}{(n!)^2} \sim \exp\left[2\sqrt{\chi(Q^2) \log(1/x_B)}\right] \quad (19.36)$$

The result in Eq. (19.36) stems from a well-known formula for the modified Bessel function I_0, which we also encountered in connection with the λ-measure, in Chapter 18.

The upshot is that in the structure functions we have a very slow Q^2-dependence $\sim \log\log Q^2$ but there is an increase for small values of x_B. From numerical studies of the DGLAP equations this increase for small x_B is confirmed. These results are quite different from the ones we obtained from the method of virtual quanta in Chapters 2 and 5. The equations do not allow a stable constant behaviour for small-x values of the combination xg and therefore neither the gluon nor the ocean $q\bar{q}$ content will behave in accordance with Feynman's speculations on the wee parton spectrum. We are evidently in a different dynamical situation!

19.5   The Lipatov results and a critique on the stability

We will show that the situation may be even worse with respect to the small-x_B behaviour in an ISB scenario investigated by Lipatov and collaborators [29] (although in the end we present some doubts on the stability of the results, which will be further enhanced in section 20.8). They show that if we keep to the leading contributions in $\log(1/x)$ then there are many subleading contributions, neglected in connection with the transverse momentum generation, which may be essential for moderate and small Q^2-values and for very small x-values. In somewhat loose language we may say that Lipatov *et al.* have investigated the possibility that the transverse momenta are not ordered as in Eq. (19.33) but may go up and down in size along the ladder. This may happen many times if the ladder is very long counted in $\log(1/x)$ units.

The results of the DGLAP as well as the BFKL approach can be reformulated (cf. Eq. (19.36)) into an integral equation relating the contribution at the nth order, G_n, to the contribution at the $(n-1)$th order, G_{n-1}:

$$G_n(x, k_\perp^2) = \int_x^1 \frac{dz}{z} \int dk_{\perp 1}^2 K(k_\perp^2, k_{\perp 1}^2) G_{n-1}(z, k_{\perp 1}^2) \qquad (19.37)$$

where the kernel K in the DGLAP case is very simple,

$$K(k_\perp^2, k_{\perp 1}^2) = \frac{\alpha_0}{k_\perp^2 \log(k_\perp^2/\Lambda_{QCD}^2)} \Theta(k_\perp^2 - k_{\perp 1}^2) \qquad (19.38)$$

It is shown in [29] that the kernel should be more complex in order to contain the possibility that the new transverse momentum, $k_\perp$, is smaller than the one before, $k_{\perp 1}$. Although the kernel is not described here (cf. Section 20.8), there is a very general mathematical result for the case when the kernel in Eq. (19.37) is symmetric.

The way to solve integral equations of this kind is to assume that it is possible to write the kernel as a (sum of) factorisable contribution(s)

$$K(k_\perp^2, k_{\perp 1}^2) = u(k_\perp^2)v(k_{\perp 1}^2) \qquad (19.39)$$

If K in Eq. (19.37) is of this form then we obtain a correspondingly factorised result for G:

$$G_n(x, k_\perp^2) = u(k_\perp^2)t_n(x) \qquad (19.40)$$

where t_n is defined by an integral (containing the eigenvalue λ):

$$t_n(x) = \lambda \int_x^1 \frac{dz}{z} t_{n-1}(z), \quad \lambda = \int dk_{\perp 1}^2 u(k_{\perp 1}^2)v(k_{\perp 1}^2) \qquad (19.41)$$

We may then iterate the equations and so obtain at the nth order of iteration

$$t_n \simeq \frac{[\lambda \log(1/x)]^n}{n!} \qquad (19.42)$$

which leads to the following small-x behaviour:

$$xg \simeq \sum t_n \sim x^{-\lambda} \qquad (19.43)$$

The kernel K in Eq. (19.37) is not factorisable in the BFKL case but there is a mathematical theorem that the eigenvalue λ and the eigenfunction u can be obtained as solutions to the following integral equation:

$$\int dk_{\perp 1}^2 K(k_\perp^2, k_{\perp 1}^2)u(k_{\perp 1}^2) = \lambda u(k_\perp^2) \qquad (19.44)$$

There are in general many such solutions but the main behaviour will stem from the largest eigenvalue, which for a constant coupling α_s is for the BFKL kernel, [29] given by

$$\lambda_{max} \equiv \lambda_L = \frac{4N_c\alpha_s \log 2}{\pi} = \frac{12\alpha_s \log 2}{\pi} \qquad (19.45)$$

(N_c is the number of colors). For $\alpha_s \simeq 0.2$ one obtains a value of $\lambda_L \simeq 0.5$.

It is of some interest to note that if we use as input a gluon structure function with $xg \sim x^{-0.5}$ then the DGLAP equations stabilise around such a behaviour also when $\log(1/x)$ becomes very large.

We also note that it is necessary to project the boundary conditions (i.e. the assumptions about the original parton wave function), onto the eigenfunction corresponding to this largest eigenvalue, λ_L. This provides a gaussian $\kappa = \log k_\perp^2$-contribution, i.e. there are some (logarithmic) transverse momentum fluctuations in the gluon emissions along the ladder that are of a gaussian character. As the length in the cascades corresponds to $\log(1/x)$ this *Brownian motion contribution* will have a width, according to BFKL, proportional to $\log(1/x)$. This is of interest with respect to the predictions of the transverse energy behaviour in the observable states in DIS. Unfortunately it seems as if the introduction of a running coupling will destroy this diffusion scenario, cf. Section 20.8.

In practice, what is done in the Lipatov treatment is to exchange a contribution stemming from the iterated integral in Eq. (19.36) for a plain number obtained in every iteration:

$$\frac{\chi(Q^2)^n}{n!} \to \lambda^n \qquad (19.46)$$

The DGLAP iteration is always directed towards larger $k_\perp$. Due to the finite available integration space it will then decrease with the number of iterations for a given top value, i.e. this contribution must diminish by a factorial. This upwards integration will always win out in the asymptotic limit when Q^2 is sufficiently large but the power may be relevant for smaller values of Q^2.

The reason for the increase in the number of small-x partons may seem rather obvious if we consider Fig. 19.5. According to the equations we are supposed to move from the right-hand lower corner in the phase-space triangle towards the point P, sampling all possible decays. In the ordinary DGLAP approach we are then supposed to move only upwards and leftwards in the shaded region. In the Lipatov treatment we are allowed to go both upwards and downwards, i.e. towards larger or smaller $k_\perp$-values, as we move to the left. This means that there are inherently more paths available in this case if we increase $\log(1/x_B)$ for a given Q^2.

The Lipatov mechanism and the BFKL effect are consistent ways to take into account some non-leading contributions but there should be corrections of the order α^2. The BFKL kernel, K, and its eigenvalues turn out to be very stable, for a constant coupling, against perturbations of the procedure. One may imagine that the (logarithmic) steps in the integration variable should be made into discrete steps (for a motivation, cf. [15] as described in section 18.6) so that Eq. (19.37) becomes a sum. This is easy to do but the results only correspond to tiny changes in the

value of λ. Mueller, [4], has also considered the production process in the transverse coordinate space and again obtains the BFKL eigenvalues from the impact parameter distributions. We will, however, end this subsection with a remark to indicate that the BFKL results are rather unstable *with respect to the non-singular terms in the z-dependence of the iteration.*

There is one feature used in the BFKL approach, i.e. that in every splitting $q' \to pq$ the virtual (gluon) propagator q contains only a *small fraction z of the energy-momentum*, while most of this energy-momentum, the fraction $1 - z$, is carried away by the emitted gluon p (we have conventionally followed the z-pole contributions and Mueller's treatment uses a corresponding motion in the rapidity $dy = dz/z$). It is then necessary for consistency to demand that the major contributions stem from regions where z is actually small, i.e. in this convention that $z < \exp(-a)$ for some real number a (which must satisfy $a > \log 2$ in order that $z < 1 - z$). If we introduce such a simple restriction into the integrations then

$$\int \prod_{j=1}^{n} dy_j \delta \left(\sum_{j=1}^{n} y_j - Y \right) \to \int \prod_{j=1}^{n} dy_j \delta \left(\sum_{j=1}^{n} y_j - (Y - na) \right)$$
$$= \frac{(Y - na)^{n-1}}{(n - 1)!} \qquad (19.47)$$

(keeping to the notation in Eqs. (19.36) and (19.35)). We have introduced the domain restriction in the expression following the arrow; the final expression summed over all values of n will no longer provide the BFKL exponential. It is straightforward, using the Stirling approximation to the factorial, to obtain the change to Eq. (19.43) as a power in $1/x$ with $\lambda_L \to \rho$, where ρ is determined by $\log(\lambda_L/\rho) = a\rho$. Thus the power in $1/x$ will be diminished so that $\lambda_L \to \rho \simeq \lambda_L(1 - a\lambda_L)$.

We conclude that *the BFKL mechanism obtains a large part of its contributions from the possibility of emitting the gluons along the ladder with moderate-to-small values of* $1 - z$, i.e. with moderate-to-large z-values. Actually this implies that one must take very many steps in order to obtain small x_B-values. One may then seriously doubt that it is allowable to neglect interference in the emissions and we will find in Section 20.8 that the QCD coherence properties are not fulfilled. We note, however, that the correction exhibited above is of order α^2 (which is expected in the BFKL treatment, and it has been repeatedly pointed out by the original authors that there should be such corrections). But it should also be noted that the correction is very large! It changes the (negative) x-power from 0.5 to about 0.3.

19.6 The CCMF model, interpolating between the DGLAP and the BFKL contributions

In this section we will consider how the DIS contributions appear in the formalism developed by Marchesini and his collaborators [44]. The ensuing model will be called the Ciafaloni-Catani-Marchesini-Fiorani (CCMF) model. This is one of the major efforts that anybody has undertaken in perturbative QCD. It was also pursued to a successful end (which has not been the case with most of the valiant efforts based upon 'good dynamics', which my generation have pursued!).

In the CCMF model there is a clever choice of the initial-state bremsstrahlung (ISB) set (p_j), which we discussed in section 19.2 in connection with the fan diagram in Fig. 19.1. (Remember also the notation, (q_j), for the propagators which connect the emission points along the fan diagram.) This choice can be described as the most general possible that is compatible with

- the QCD coherence conditions (the strong angular ordering, as described in Chapter 17)

- energy-momentum conservation, as implied by Eq. (19.1), and the possibility of keeping the (p_j) massless.

All emissions are ordered in rapidity, which (due to the relation between angle and rapidity, i.e. for a massless particle $y = \log \cot(\theta/2)$ with θ the ordering angle) means *strong angular ordering* along the chain, i.e. that the QCD coherence conditions are fulfilled. The CCMF model then picks the ISB set (p_j), from the set of all emissions, as those emissions each of which is *not* followed (in the rapidity ordering variable) by another one with a larger lightcone energy-momentum p_+ $(= p_0 + p_3 \equiv p_\perp \exp y)$. In this way the chosen p_j has a larger 'energy' than the rest and one may, in the leading-log approximation (LLA), neglect the recoils from the emission of the final-state bremsstrahlung (FSB).

More precisely, in terms of the ordinary variables $z_j, \mathbf{p}_{\perp j}$ with $q_{+j} = z_j q_{+(j-1)}$ and $\mathbf{q}_{\perp j} = \mathbf{q}_{\perp(j-1)} - \mathbf{p}_{\perp j}$, the CCMF choice for the q_+ implies (in the LLA) that $q_{+j} \ll q_{+(j-1)}$. Therefore the splitting function is again approximated as $\mathscr{P}(z) \propto 1/z$ so that z is small enough for the approximate relation $1 - z \simeq 1$ to hold, which means that $p_{+j} = q_{+(j-1)}(1-z_j) \simeq q_{+(j-1)}$. Further, the gluons in the sets $(h)_j$ are, in accordance with the LLA, treated as soft enough that the p-vectors can be taken as on-shell and massless but the propagator vectors q are all spacelike. The transverse momenta of the propagators $q_\perp$ are dominated by the $p_\perp$-emissions in the neighborhood, see below. A major kinematical constraint is

$$q_{\perp j}^2 > z_j p_{\perp j}^2 \tag{19.48}$$

If this is not fulfilled then the virtuality of the propagator will, in the LLA, fulfil $|q^2| \gg q_\perp^2$, which implies strong suppression. Each step in the emission chain is, in the CCMF model, described by the weight

$$\bar{\alpha} \left(\frac{dz_j}{z_j} \right) \frac{dq_{\perp j}^2}{q_{\perp j}^2} \Delta_{NE}(z_j, q_{\perp j}, p_{\perp j}) \qquad (19.49)$$

Here $\bar{\alpha}$ is the effective coupling (including color factors) and Δ_{NE} is the so-called 'non-eikonal form factor', with

$$\Delta_{NE}(z_j, q_{\perp j}, p_{\perp j}) = \exp[-\bar{\alpha} \log(1/z_j) \log(q_{\perp j}^2/z_j p_{\perp j}^2)] \qquad (19.50)$$

The first major result in the CCMF model is this non-eikonal form factor, corresponding to the radiative corrections for the choice of the ISB set defined above (for the second, i.e. the fact that there are no FSB emissions with $p_\perp^2 > -q^2$, see below). We note in particular that due to the properties of this form factor small values of z_j and $p_{\perp j}$ in Eq. (19.49) are effectively cut off if we assume that $q_{\perp j}$ is finite.

The negative exponential in the non-eikonal form factor corresponds to an area multiplied by the effective coupling $\bar{\alpha}$. We will end this section with a description of this area (and some associated ones) and show that we may interpret the occurrence of the non-eikonal form factor just as an ordinary Sudakov factor, i.e. there is a region excluded for gluon emissions because of the particular choice of ISB in the CCMF model.

In Fig. 19.7 a set of gluon emissions is shown, denoted from the hadron front end $a, b, 1, c, 2, d, 3$. The gluons denoted by the numbers $1, 2, 3$ fulfil the requirements for the ISB gluons in the CCMF model and in each case there are surfaces Aj, Bj, Cj exhibited (in between the consecutive gluons). The gluons denoted by letters, however, are all FSB gluons, i.e. they do not fulfil the CCMF conditions of rapidity and p_+-ordering necessary for ISB gluons. Note that the gluons denoted a, b are followed in rapidity by $p_{+1} > p_{+a}, p_{+b}$, gluon c by $p_{+2} > p_{+c}$ and gluon d by $p_{+3} > p_{+d}$. Actually all possible gluons inside the three regions denoted $Aj, j = 1, 2, 3$, in the figure are FSB gluons in the CCMF model, i.e. the gluons occurring inside the regions Aj may, according to the rules of the CCMF model, be emitted in connection with the ISB gluon j.

To understand the relationship between these surfaces and the non-eikonal form factor we start with the transverse momentum properties of the emissions. From the relationship $\mathbf{q}_{\perp j} = \mathbf{q}_{\perp j-1} - \mathbf{p}_{\perp j}$ we obtain in the leading-log approximation that there are three possible situations:

T1 $\mathbf{p}_{\perp j}^2 \simeq \mathbf{q}_{\perp j}^2 \gg \mathbf{q}_{\perp j-1}^2$, i.e. the propagator transverse momentum increases owing to the emission;

T2 $\mathbf{q}_{\perp j}^2 \simeq \mathbf{q}_{\perp j-1}^2 \gg \mathbf{p}_{\perp j}^2$, i.e. the emitted gluon momentum is much smaller so that the propagator retains its momentum in such a step;
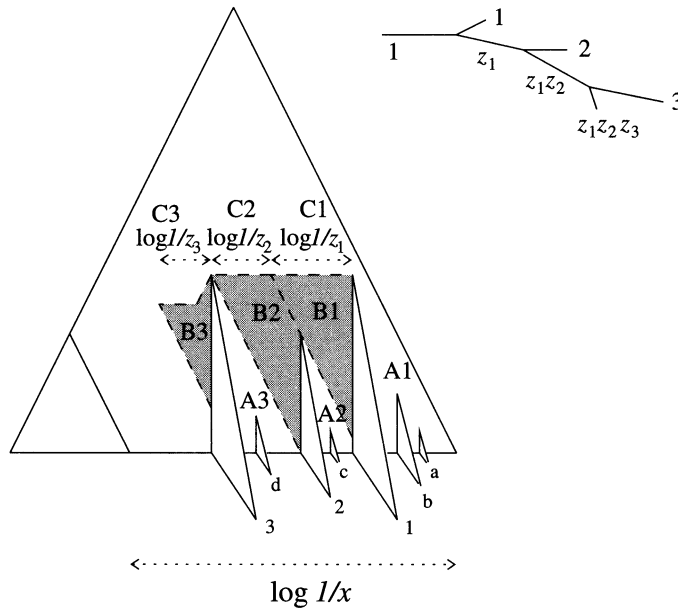
Fig. 19.7. Examples of gluon emissions in the CCMF model with the associated areas Aj, Bj, Cj. The notation is defined in the text.

T3 $\mathbf{q}_{\perp j-1}^2 \simeq \mathbf{p}_{\perp j}^2 \gg \mathbf{q}_{\perp j}^2$, i.e. as the emitted gluon picks up most of the momentum of the incoming propagator (index $j-1$) the momentum of the outgoing propagator (index j) goes down.

In Fig. 19.7 the examples are chosen so that emission j corresponds to case Tj above. There are, besides the surfaces Bj, also regions Aj and Cj and we note that the upper boundaries of the regions Bj (corresponding to the lower boundary of the regions Cj) each correspond to a measure of the relevant propagator transverse momentum, to be precise to $\log q_{\perp j}^2$. We have also indicated the distances $\log(1/z_j)$ in each step. We will now investigate the negative exponential of the non-eikonal form factor using these examples. We will find that it corresponds to (besides the effective coupling $\bar{\alpha}$) *the size of the regions Bj in phase space which are excluded due to this particular choice of ISB.*

We firstly note that there are no emissions inside the regions denoted Cj. It is shown in the CCMF model that *inside these regions there can be no emissions because the real emissions are just cancelled by the virtual corrections.* Although this statement is hardly noticeable for the results in Eq. (19.50) it is arguably the major result of the CCMF model (and is very difficult to prove!). We will provide a dynamical reason for this

feature in Chapter 20 in connection with the linked dipole chain model, [16]. But we note that its practical implication is that there can be no FSB emissions for values of gluon transverse momentum above the corresponding propagator transverse momentum.

We now note that for the emission of the ISB gluon 1, corresponding to the case $T1$ defined above, we have according to the formula for the non-eikonal form factor a negative exponential of $\log^2(1/z_1)$ (note that $\mathbf{p}_{\perp 1}^2 \simeq \mathbf{q}_{\perp 1}^2$) and according to Fig. 19.7 this is just the size of area $B1$.

It is evident that for gluons emitted in the region $B1$ it is impossible to fulfil both the angular condition and energy-momentum conservation. In particular, to conserve the p_+-component such gluons cannot be sent out from the 'next' gluon, 2, but at the same time neither can they, according to the rules of the CCMF model, be treated as FSB gluons with respect to gluon 1, because of the rapidity ordering.

In connection with the emission of gluon 2, corresponding to the case $T2$, the negative exponential of the form factor contains, besides the same factor $\log^2(1/z_2)$ as that occurring for $T1$, a further factor $\log(1/z_2)\log(q_{\perp 2}^2/p_{\perp 2}^2)$ and it is easy to see that the two factors together make up the surface area of $B2$ (Fig. 19.7). The reason why there can be no gluon emission inside the region $B2$ is essentially the same as for $B1$, i.e. the rapidity ordering of the CCMF model forbids the region 'behind' gluon 2, while energy-momentum conservation does not allow these gluons to be emitted by the next ISB gluon, 3.

Finally, for the emission of gluon 3, we note the combined effects of the constraint in Eq. (19.48) and the fact mentioned above that the region $C3$ is (in the LLA) a strictly forbidden emission region. This means that due to Eq (19.48) there can be no gluon emission in front of the negative lightcone line of p_{-3} and above the new propagator transverse momentum $k_{\perp 3}$. The size of the area $B3$ again equals the (negative) logarithm of the non-eikonal form factor.

We may remark explicitly that although the total state weight in the CCMF model, given by the allowed ISB gluon phase space multiplied by the non-eikonal form factor, contains recognition of only the surface areas B_j (which must be empty due to the particular choice of ISB in the model) the regions A_j are not forgotten. Inside these regions any number of FSB gluons may be emitted in a state defined by the ISB gluons. All these emissions can be summed up so that the weight becomes 1. For any particular exclusive state, however, there will of course be a Sudakov factor, corresponding to the regions not used in that state.

It is possible, in accordance with [44], to write out integral equations for the structure functions in the CCMF model and, as we may expect, these equations will have solutions with behaviour in between the DGLAP and the BFKL results. The equations are, however, somewhat complicated and

it is difficult to use them in connection with a Monte Carlo simulation. The reason is that to make it into a consistent stochastical process it is necessary to keep track of the constraints in z, rapidity (with respect to the earlier emission), $p_\perp$ and $q_\perp$. In Chapter 20 we will present a generalisation of the CCMF model, the linked dipole chain model, in which both the weight distributions and the Sudakov factors are simpler so that the implementation in terms of a Monte Carlo simulation process is straightforward.

19.7   The GLR model of reinteraction of partons

The basic idea in the GLR model is that if the number of gluons becomes very large then the partons will be very closely packed inside the proton. There will then be a correspondingly large probability for them to reinteract.

In order to find when this starts to happen we will use the arguments of Gribov, Levin and Ruskin, [67]. They noted that the number of gluons per unit rapidity is given by $dn_g/dy = xg$. If all these gluons are inside a transverse (impact parameter) region πR^2 then the average surface density is $xg/(\pi R^2)$. Further, the gluonic cross section at a given value of Q^2 is $\sigma_g \sim \alpha_s(Q^2)/Q^2$ and therefore it was concluded in [67] that the crucial parameter for a possible reinteraction is

$$\Omega(x, Q^2) = \frac{\alpha_s(Q^2)xg}{Q^2\pi R^2} \tag{19.51}$$

As long as the parameter Ω is very small the ordinary DGLAP equations (provided with the proper angular ordering) are expected to work. But, for sufficiently small values of x, when xg becomes large two gluons from different cascade chains may interact thereby fusing the different ladders and decreasing the total multiplicity.

The authors of [67] have been able to take into account such two-body interactions, cf. also [95]. The result is that the DGLAP equation for the gluon distribution obtains a negative contribution

$$\frac{dg}{d\tau} = \alpha_s \int_x^1 \frac{dz}{z} \left[\sum_i^{2n_f} \mathscr{P}_g^{q_i}\left(\frac{x}{z}\right) q_i(z,\tau) + \mathscr{P}_g^g\left(\frac{x}{z}\right) g(z,\tau) \right] - I$$
$$I = \frac{81\alpha_s^2(Q^2)}{16R^2Q^2x} \int_x^1 \frac{dz}{z} [zg(z,Q^2)]^2 \tag{19.52}$$

This contains a non-linear contribution in which the square of the gluon structure function occurs together with a set of color factors and finally an unknown size parameter, R, with the dimension of length. The meaning

of R is that it comes from the integral over the transverse region inside which the interaction takes place.

It is pointed out in [95] that if $R \sim 1$ fm, the approximate proton radius, then the correction term is very tiny indeed and will not play any role for the HERA region.

This has lead to some speculation that inside the proton there may be more or less dense subregions and that the correction term may play a large role in such a dense and small subregion, a 'hot spot'. We will, however, not pursue the question any further in this book.